

Selective dissolution of magnetic iron oxides with the acid-ammonium-oxalate/ferrous-iron extraction technique—II. Natural loess and palaeosol samples

I. H. M. van Oorschot,¹ M. J. Dekkers¹ and P. Havlicek²

¹Utrecht University, Palaeomagnetic laboratory Fort Hoofddijk, Budapestlaan 17, 3584 CD Utrecht, The Netherlands. E-mail: dekkers@geo.uu.nl

²Czech Geological Survey, Klarov 3, 118 21 Prague 1, Czech Republic

Accepted 2001 October 8. Received 2001 September 19; in original form 2001 March 5

SUMMARY

Chemical extraction techniques are being introduced into environmental magnetism studies to aid in the interpretation of magnetic climate proxies. Previous studies have shown that the acid-ammonium-oxalate/ferrous-iron (AAO-Fe²⁺) extraction technique can be used to selectively dissolve very fine-grained magnetite and maghemite from synthetic samples. Here, we present the results of a study of this extraction technique to serve as a tool for selective dissolution of pedogenic magnetic minerals from a loess–palaeosol transect. Before and after extraction, the samples were subjected to classic mineral–magnetic methods (measurement of low-field susceptibility and hysteresis parameters), as well as first-order reversal-curve analysis. In addition, acquisition curves of the isothermal remnant magnetization (IRM) were fitted with logarithmic distributions. These analyses showed the magnetic dominance of low-coercivity magnetic minerals. By subtracting the IRM remaining after extraction from that before extraction, the magnetic fraction that was dissolved could be characterized as well, supplying extra information concerning the performance of the extraction technique.

The AAO-Fe²⁺ method successfully dissolved the superparamagnetic and part of the single-domain material from the palaeosol samples in one extraction step, repeating the extraction resulted in hardly any further changes to the magnetic content of the samples. The magnetic characteristics of the loess samples remained stable throughout the extraction experiment. The combination of the AAO-Fe²⁺ extraction with mineral–magnetic analysis has successfully identified the pedogenic contribution in our samples. Therefore, variations in the lithogenic fraction potentially present in pedogenically enhanced intervals can be assessed, improving the merit of mineral–magnetic climate proxy parameters.

Key words: environmental magnetism, extraction techniques, loess–palaeosol sequences, rock magnetism, South Moravia.

INTRODUCTION

Loess–palaeosol sequences have been the topic of many investigations over the past decades. The focus of most studies was originally on determining the (magneto) stratigraphy and correlation with other terrestrial and marine sequences (Busacca 1989; Maher 1998; Zhou & Shackleton 1999), and later turned to the mineral–magnetic parameters that reveal the climatic history contained in the sequences (Heller & Liu 1986; Singer & Fine 1989; Liu *et al.* 1998; Fang *et al.* 1999). Understanding the type of magnetic minerals and the grain-size fraction that carry the climatic information, will help constrain the interpretation of the magnetic climate proxies.

Several studies have shown that some magnetic parameters, such as the low-field susceptibility, correlate with the oxygen isotope curve, therefore they can be used as climate proxies (Kukla 1987;

Kukla *et al.* 1990; Heller & Evans 1995; Maher 1998; Liu *et al.* 1998). However, the interpretation of this correlation may be ambiguous, because in some geographical locations the magnetic signal in palaeosols is enhanced compared with that of the loess (such as the sequences in China and Central Europe), while in other locations the reverse is true (for example, in sequences in Siberia and Argentina; see Maher 1998).

The magnetic particles in loess are, in principle, deposited at the same time as the loess itself, and therefore give information concerning the source area of the loess. However, chemical alteration (such as oxidation) of the magnetic minerals in the loess after deposition cannot be ruled out (Maher 1998). In contrast, the palaeosols have a complicated magnetic signal—it originates partly from the original magnetic minerals in the loess and partly from the magnetic particles formed and/or chemically altered during pedogenesis (e.g. by

chemical and bacterial processes as well as natural fire (Kletetschka & Banerjee 1995; Cornell & Schwertmann 1996). Extensive pedogenesis may even downprint the palaeomagnetic signal by 1000 years or more (Zhou & Shackleton 1999; Heslop *et al.* 2000). In the case of magnetically enhanced palaeosols, it is therefore necessary to differentiate between the lithogenic and pedogenic contribution of the magnetic signal to extract the most meaningful climatic information from palaeosols. Subtraction of the magnetic signal from adjacent loess intervals may lead to erroneous conclusions, because the pedogenic signal is not uniquely based on neoformation of magnetic particles but also on the transformation of existing lithogenic particles. Furthermore, the composition of the loess may have varied throughout deposition.

To identify the link between magnetic properties and climate change, an interpretation based on mineral–magnetic information only, is often insufficiently distinctive, and complementary techniques such as citrate–bicarbonate–dithionite (CBD) extraction methods have been introduced to help constrain the interpretation (Singer *et al.* 1995; Hunt *et al.* 1995). By dissolving the small particles, chemical extraction techniques may offer supplementary information on the changes that have taken place in the lithogenic fraction during the formation of the palaeosols. A number of extraction techniques have been investigated in the past to determine the dissolution behaviour of fine- and coarse-grained iron oxides and to find the most suitable technique for the specific question at hand (Singer *et al.* 1995; Hunt *et al.* 1995; van Oorschot & Dekkers 1999, 2001). The acid-ammonium-oxalate/ferrous-iron (AAO–Fe²⁺) extraction technique has yielded promising results in synthetic samples (van Oorschot & Dekkers 2001). The method readily dissolves fine-grained iron oxides (<0.5 µm), and attacks maghemite preferentially over magnetite. Furthermore, the results are not dependent on the concentration of magnetic iron oxides, which seems to be the case with the CBD extraction when the amount of iron oxides is high (van Oorschot & Dekkers 1999). In natural samples the AAO–Fe²⁺ technique is expected to preferentially dissolve the smaller magnetic particles (<0.5 µm) from the sample, leaving behind the coarse-grained particles that are of lithogenic origin. With magnetic analysis of samples before and after chemical extraction, more information can be obtained concerning possible alterations of the original lithogenic particles in the palaeosol.

Here, we aim to compare the results of the AAO–Fe²⁺ extraction method for natural samples with a directly related study into the dissolution behaviour of synthetic samples (van Oorschot & Dekkers 2001), to see whether these behave in a similar way. The dissolution behaviour of magnetic minerals from a loess–palaeosol sequence from South Moravia (Czech Republic) during treatment with the AAO–Fe²⁺ extraction method will be discussed. Besides conventional rock-magnetic techniques, two new methods are incorporated into our study; first-order reversal-curve (FORC) (Pike *et al.* 1999; Roberts *et al.* 2000) and automated isothermal remanent magnetization (IRM) component analysis (Kruiver *et al.* 2001; Heslop *et al.* 2002). In this way we obtained detailed information of the effects of the extraction technique on the composition and grain-size distribution of magnetic minerals in our samples.

MATERIAL AND METHODS

Loess–palaeosol sequences of Central Europe

Loess–palaeosol sequences of the Quaternary age occur sporadically over a wide area in Europe, from sites in Normandy (France)

to deposits as far east as the Ukraine (Stemme 1998). In South Moravia, where the Czech Republic borders Austria and Slovakia, loess–palaeosol sequences are abundant. The loess was deposited during the glacial phases of the Pleistocene. During the interglacial stages the climate became warmer and rainfall increased, this enabled soils to develop in the top of the loess deposits. Usually, during the following glacial stage the top of the newly formed soils was partly eroded and the soils were subsequently buried by younger loess deposits (Kraus 1999). These fossil soils are referred to as palaeosols, and Rotlehm, Braunlehm and Chernozem soils are the most common types of palaeosol found in Moravia (classification according to Kubierna and Mückenhausen in Kuntze *et al.* 1981).

The sequences in Moravia are grouped into soil complexes (also known as pedocomplexes or PK), with each complex representing a complete glacial–interglacial cycle. The soil complexes can contain more than one loess/palaeosol sequence. For example, soil complex PK IV dates from oxygen isotope stage 7, and is usually distinguished by a double pedocomplex consisting of a pair of lower reddish-brown Bt horizons (Parabraunerde) overlain by Chernozems, and these soils are intercalated by loess or redeposited loess (Frechen *et al.* 1999).

Sample location

We sampled a site of well-developed loess with several palaeosols just north of the village of Bořetice (Fig. 1). This site contains four palaeosols, each developed at a different time. The top of the section has been partly disturbed by solifluction, therefore we only sampled the lowermost, oldest palaeosol and the loess underneath it. The sampled section is represented schematically in Fig. 2—a trench was dug to obtain fresh samples. The top part of the sampled section consists of an earthified Rotlehm, which formed from the loess during the Lower–Middle Pleistocene (~0.9 to ~0.5 Myr) close to the Matuyama/Bruhnes boundary, it has been identified as belonging to soil complex PK VII. The lower part of the section contains the original loess and dates from the Lower Pleistocene (Havlicek & Smolikova 1993). The A-horizon of the palaeosol has been eroded prior to the new deposition of loess. The magnetic enhancement in the palaeosol is therefore most probably the result of precipitation of iron that has been dissolved from the minerals in the topsoil and transported downward. Bulk susceptibility and colour were measured in the field at 2.5 and 5 cm intervals, respectively,

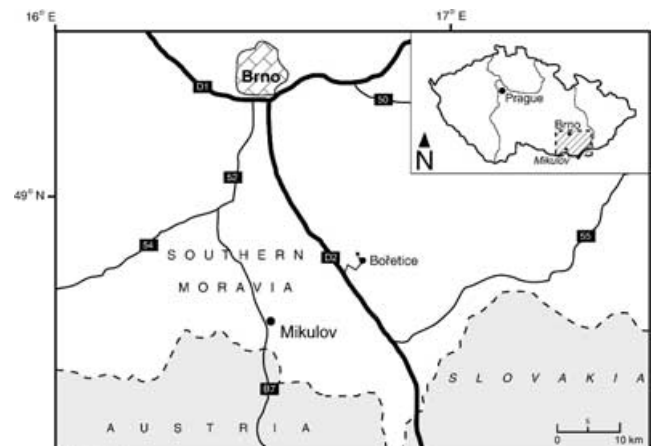


Figure 1. Geographical map showing the site location. The site is located at ~40 km SSE of Brno, just North of the town of Bořetice.

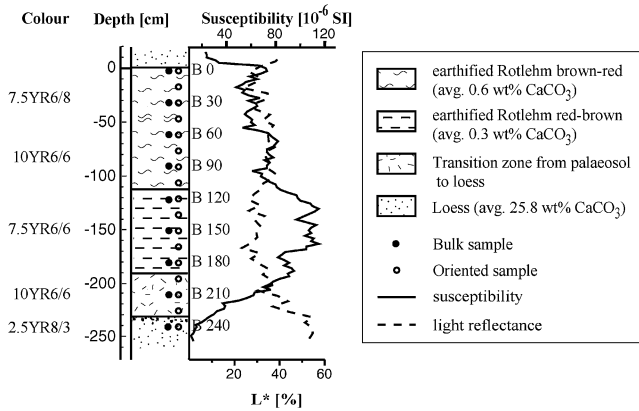


Figure 2. Schematic representation of the sampled section. Colour indications are according to the Munsell notation. The sampled levels are indicated with open circles (oriented samples) and closed circles (bulk samples). The susceptibility was measured in the field (every 2.5 cm) and is represented by the solid line and light reflectance (every 5 cm) is represented by the dashed line. There is a gradual change from the loess horizon towards the enhanced palaeosol between -230 and -190 cm depth. The carbonate contents are averages of the top of the palaeosol and the lower (most enhanced) part of the palaeosol with two samples measured for each sampled level. The standard deviation in the carbonate content was 0.1 per cent for all samples.

with a Bartington MS2F probe (sensitivity of 2×10^{-6} SI) and a Minolta CM508i portable spectrophotometer.

Samples

Bulk samples, to be extracted chemically, were taken at 30 cm intervals by digging into the surface of the trench and collecting the fresh material in plastic. To check whether the Matuyama–Brunhes boundary had been recorded in this section, oriented samples were taken every 15 cm by carefully pressing plastic cylinders with orientation marks into the surface of the section (samples were coded BxxA, with xx signifying the sample depth). The plastic cylinders (taking 8 cm^3 of sample) were similar in size to standard palaeomagnetic samples (outer dimensions: 25 mm diameter and 22 mm height). Prior to analysis, the oriented samples were stored in a refrigerator (at 4°C). The bulk samples were dried in air for 24 h, and then stored in a refrigerator.

The bulk material was powdered with a pestle and mortar, and subsamples were taken for various analyses. For the extraction experiments, a sample series consisted of three 1.00 g samples from the same level in the section as well as one blank sample consisting of pure quartz (Merck, analytical grade) were used. For the carbonate analysis, 0.5–1 g of sample was used, from each level two subsamples were analysed. The bulk material was also subsampled for IRM acquisition analysis. These samples (1–2 g) were weighed into plastic cylindrical cups (the same as those used to take oriented samples in the field) and mixed with epoxy resin (Araldit D, Hardener HY956, Ciba Speciality Chemicals). FORC analysis requires much smaller samples dictated by the sample probe of the MicroMag. Powdered samples containing typically 10 mg of sample material were mixed with the epoxy resin and cast in Teflon moulds, which resulted in cylindrical samples with a diameter of ~ 1.5 mm and a length of maximum ~ 2 mm. Some of the extracted samples carried only a very weak magnetic signal, these were cast in a mould with a diameter of ~ 4.5 mm and a length of maximum

~ 4 mm (containing ~ 50 mg of sample material) to improve data acquisition with the magnetometer.

Chemical analyses

The calcium carbonate content of the samples was determined with a Scheibler analyser, it involves the addition of 7 ml of 1 M hydrochloric acid solution to a weighed amount of sample. The volume of CO_2 gas that is formed during the dissolution of calcium carbonate in the acid is used to determine the calcium carbonate content of the sample.

The AAO– Fe^{2+} extraction technique has been described in detail by van Oorschot & Dekkers (2001). It uses a 20 mM acid ammonium oxalate solution with 2 mM ferrous iron added at a pH of 3. The extraction solution is prepared using deoxygenated water to prevent precipitation of the iron during the preparation and the extraction experiment. For each sample, 50 ml of this solution is required to perform one extraction step, and a fresh solution is prepared for each extraction step. The containers (vials made of brown glass) with the samples and the extraction solution are placed on a mechanical shaker at room temperature and at medium speed for 30 min. Aluminium foil is wrapped around the containers and the shaker to prevent photochemical dissolution. After 30 min the liquid and solid phase are separated by centrifuging for 15 min at 3600 g (~ 4417 rpm). The samples are rinsed with ~ 50 ml deionized water and centrifuged again. The remaining solid is dried in an oven at 40°C for ~ 12 h. The extraction step is repeated a maximum of two times, with each sample series requiring 1 day for extraction and drying of the samples.

Magnetic measurements

The natural remnant magnetization (NRM) of the oriented samples was measured with a 2G Enterprises DC SQUID magnetometer (noise level 4×10^{-12} A m^2). Stationary three-axis AF demagnetization was performed in a laboratory-built coil with a maximum peak field of 300 mT. We used a maximum demagnetization field of 250 mT. The oriented samples were also used to measure the frequency dependence of the low-field susceptibility (χ_{fd}) on a Bartington MS2B dual-frequency sensor (with a low frequency of 460 Hz and a high frequency of 4600 Hz; sensitivity 2.5×10^{-6} SI). Thermomagnetic analysis was performed in air with a modified horizontal translation-type Curie balance.

Prior to the start of the extraction experiment and after each extraction step, the dry samples are weighed and bulk susceptibility as well as hysteresis parameters of the samples were measured. The bulk susceptibility (χ_{in}) was measured with a KLY-2 bridge-type susceptometer (AGICO). The sensitivity of the equipment was 4×10^{-8} SI, and our data were at least two orders of magnitude higher. The hysteresis loops were measured with an alternating gradient magnetometer (MicroMag) with a saturation field of 500 mT and a field increment of 5 mT. At 500 mT all samples appeared to be magnetically saturated. The sensitivity of the micromagnetometer is 1×10^{-9} A m^2 , which is at least two orders of magnitude lower than the magnetization of our samples. All measurements were 70 per cent slope corrected because of the high diamagnetic signal. Backfield demagnetization was performed in the same magnetometer with a field increment of 1 mT to a maximum field of -100 mT to determine the coercivity of the remanence.

IRM was induced using a PM4 pulse magnetizer and measured with a JR5A spinner magnetometer (AGICO). The sensitivity of the

spinner magnetometer is $\sim 2.7 \times 10^{-11} \text{ A m}^2$ and the minimum IRM measured during our experiments was at least twice as strong. IRM acquisition curves (completely saturated) were analysed using the cumulative log Gaussian (CLG) program of Kruiver *et al.* (2001) and the automated analysis method of Heslop *et al.* (2002) to determine magnetic coercivity components in the samples. This involves fitting a measured IRM acquisition curve with a number of logarithmically distributed coercivity distributions, each characterized by their midpoint ($B_{1/2}$), spreading or dispersion, and magnetic concentration. A statistical test is provided to determine the number of distributions required for an optimal fit. The fitting was also performed for the samples that had been extracted. The data were subsequently mass-corrected and subtracted, taking into account the small but slightly varying contribution of the epoxy resin. The resulting IRM curve was analysed using the same programs and represents the grains that had been dissolved with the extraction technique. The grain-size variations of the magnetic minerals in the samples before and after extraction were also studied using FORC analysis (Pike *et al.* 1999). Data acquisition was performed on the alternating gradient magnetometer.

RESULTS

Susceptibility of the profile and carbonate content of the original samples

The low-field susceptibility is enhanced in the lower part of the Rotlehm compared with that of the loess, which is consistent with the observation that all central European palaeosols have an enhanced susceptibility (Sartori *et al.* 1999). The average carbonate content in

the palaeosol is ~ 0.5 wt per cent, the loess horizon has an average carbonate content of ~ 26 wt per cent.

Magnetic characterization of original samples

Curie balance

The thermomagnetic data all show that the samples contain (slightly cation-deficient) magnetite ($T_C = 590^\circ \text{C}$) which oxidizes upon heating to 700°C (not shown). The magnetization at room temperature is low, and indicates a small concentration of magnetite in all samples. In the loess samples the signal is particularly weak.

NRM

Because the palaeosol was formed during the Middle Pleistocene, the Matuyama/Bruhnes boundary may have been recorded in this section. However, the NRM data show that all samples have normal polarity (Fig. 3A); thus the boundary was not recorded in this section. The type of NRM in the section varies, in the soil where existing minerals may have been altered (e.g. by oxidation) and new minerals may have precipitated and the remnant magnetization presumably has a chemical nature (CRM or chemical remnant magnetization). The chemical remanence was most probably formed during soil formation, because during that period chemical reactions take place which dissolve and form iron oxides. In the loess the NRM was mostly formed during the deposition of the loess particles and therefore it may be taken as being some form of detrital remnant magnetization (DRM).

AF demagnetization revealed that most samples have a two-component NRM. In these samples a viscous overprint (presumably

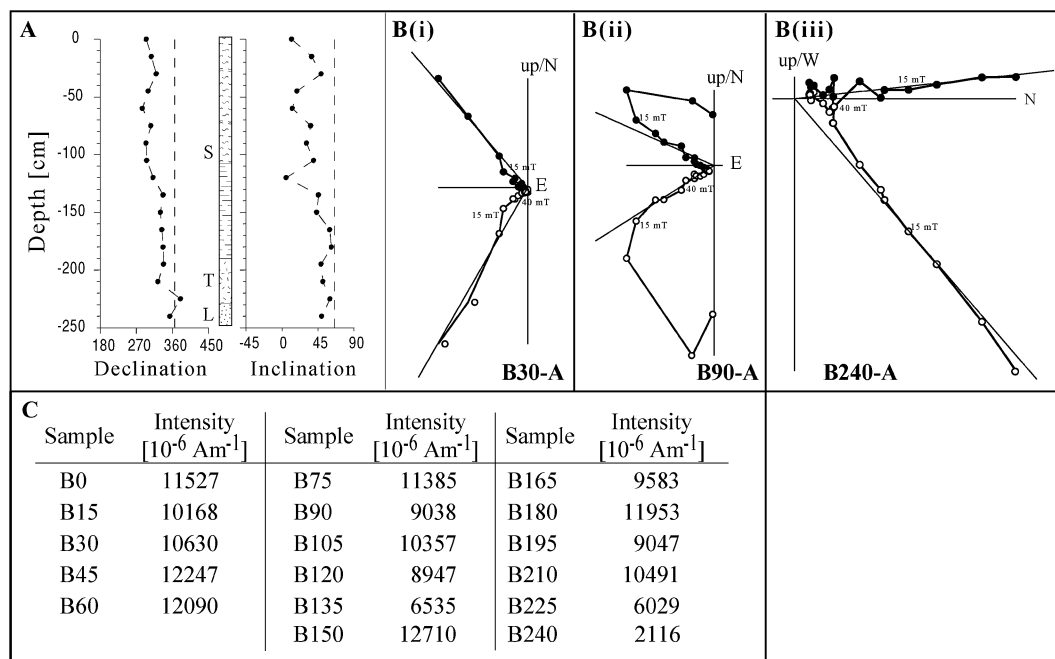


Figure 3. NRM for the oriented samples, AF demagnetization was induced with fields of 5, 10, 15, 20, 25, 30, 35, 40, 50, 60, 80, 100, 150, 200 and 250 mT. Panel A gives declination and inclination throughout the section, the dashed lines represent the declination and inclination of the present geocentric axial dipole field for the site. The lithology of the sampled section is schematized in the column of panel A. Here, S indicates the palaeosol, L is the loess and T is the transitional zone between palaeosol and loess. Panels B(i)–(iii) are Zijderveld diagrams of typical examples from the section. Closed (open) symbols represent projection to the horizontal (vertical) plane. All samples have a normal polarity NRM (panels B(i) and (iii) from the palaeosol and the loess, respectively), while some samples show a viscous overprint presumably acquired during storage (panel B(ii)). The original intensity of the samples is given in the table (panel C).

by the laboratory field) is displayed by the low-coercivity NRM fraction (B90-A in Fig. 3B(ii) is an example). Viscous overprints are only found in the palaeosol (0 to -180 cm), with the exception of sample B30 and the samples from the transition zone and the loess (-180 to -240 cm), which has only a one-component NRM tending toward the origin. The viscous overprint in the palaeosol suggests a higher concentration of small SD grains (close to the SD-SP boundary) in this part of the profile.

The intensity of the samples before AF demagnetization was approximately constant throughout the section (~ 9 to $\sim 12 \times 10^{-3}$ A m $^{-1}$) except for the bottom of the section (loess samples) which had a lower intensity (2×10^{-3} A m $^{-1}$). After demagnetization to 250 mT the average remaining intensity of the samples is $\sim 0.7 \times 10^{-3}$ A m $^{-1}$, but for the lower part of the section this value is even smaller (0.1×10^{-3} A m $^{-1}$).

The NRM that remains after AF demagnetization at 100 mT is an indication of the presence of hard magnetic components such as haematite or goethite. The samples between 0 to -50 cm and ~ -165 to -210 cm are completely demagnetized at fields of 30-40 mT (99 per cent of their initial NRM intensity is lost). The palaeosol samples between -50 and -165 cm require 100 mT to be completely demagnetized (99 per cent of their initial NRM intensity is lost). The loess samples require AF demagnetization at fields of 60-80 mT. In most samples the NRM decays in a two-stage fashion with a plateau at 40-60 mT (the NRM intensity at this field range is $\sim 1-2 \times 10^{-3}$ A m $^{-1}$).

Low-field susceptibility

χ_{in} ranges between $\sim 500 \times 10^{-9}$ m 3 kg $^{-1}$ in the most enhanced parts of the palaeosol to $\sim 100 \times 10^{-9}$ m 3 kg $^{-1}$ in the loess (Fig. 4). Within the palaeosol, χ_{in} varies with depth. From 0 to ~ -100 cm, χ_{in} is enhanced compared with that of the loess, between ~ -100 and ~ -200 cm, the enhancement is even more pronounced. Between ~ -190 and ~ -230 cm the transition from palaeosol to loess occurs, this is reflected in a strong decrease in χ_{in} . The χ_{in} pattern found in the field matches that of χ_{in} measured in the laboratory (Fig. 4). The χ_{fd} measurements (Table 1) show that the concentration of SP grains in the palaeosol is higher than that of the loess

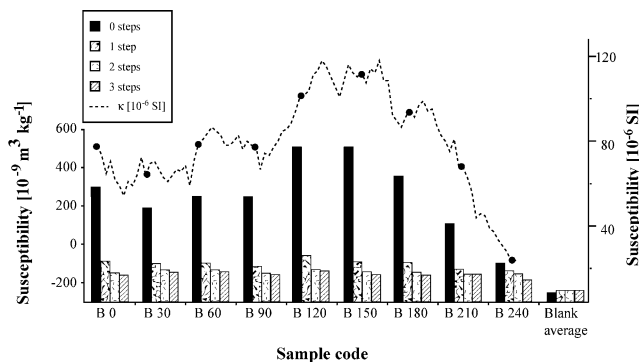


Figure 4. Susceptibility change of samples subjected to the AAO-Fe $^{2+}$ extraction method. The bars give the susceptibility of the bulk samples before and after extraction (corrected for sample holder). The black bars represent samples that have not been extracted. The numbers in the legend refer to the number of extraction steps performed (an average of three samples per horizon, with data for the blanks based on nine samples (one for each sampled level)). The dotted line represents the bulk susceptibility as measured in the field, with the closed circles indicating the level at which each bulk sample was taken.

Table 1. The frequency dependence of the low-field susceptibility of the unextracted, oriented samples. The loess level is represented by sample -240 cm, while the gradual change from loess to palaeosol is represented by samples -195 to -225 cm.

Sample	Frequency dependence $((\kappa_{lf} - \kappa_{hf}) \times 100) / \kappa_{lf}$ (per cent)	Absolute difference in frequency susceptibility $(\kappa_{lf} - \kappa_{hf})$
B0	10.0	7.2
B15	10.4	5.9
B30	9.5	5.3
B45	9.8	5
B60	9.9	6.9
B75	8.8	5.6
B90	9.2	5.9
B105	9.4	6
B120	10.2	9.5
B135	10.1	10.1
B150	10.4	9.1
B165	10.2	8.7
B180	9.7	7.2
B195	9.0	6
B210	9.1	4.3
B225	7.9	2.5
B240	3.7	0.5

samples (χ_{fd} is, respectively, ~ 10 and 4 per cent). These values correspond with those of other studies of natural soils. Magnetically most enhanced soils have χ_{fd} in the range of 4-12 per cent, while the C horizon usually has $\chi_{fd} \sim 0-4$ per cent (Maher 1998; Hanesch & Petersen 1999). The origin of the SP grains is most probably the precipitation of iron (for example, as haematite pigment) that was dissolved in the topsoil and has migrated downward in the soil profile. SP grains have a much higher susceptibility than coarser grains (Thompson & Oldfield 1986; Dunlop & Özdemir 1997), therefore, the enhanced χ_{in} in the soils originates at least in part from the presence of haematite pigment, while the main part of the increased χ_{in} originates from the increased concentration of SD-like spinel iron oxides.

Hysteresis parameters

All samples have a magnetization ratio (M_{rs}/M_s) of 0.1-0.2, and a coercivity ratio (B_{cr}/B_c) of 3-4 (Table 2), which means they plot in the pseudo-single-domain (PSD) region of the Day plot, close to the multidomain (MD) field (Day *et al.* 1977). The 'grain size'

Table 2. Change in magnetization ratio (M_{rs}/M_s) and coercivity ratio (B_{cr}/B_c) for the samples before and after extraction with the AAO-Fe $^{2+}$ method. 0 = before extraction, 1 to 3 after the respective extraction steps.

Code	M_{rs}/M_s				B_{cr}/B_c				
	0	1	2	3	Code	0	1	2	3
B0	0.14	0.18	0.17	0.15	B0	4.0	3.2	3.7	4.6
B30	0.15	0.14	0.25	0.18	B30	3.7	3.6	3.3	4.3
B60	0.16	0.13	0.19	0.16	B60	3.4	3.7	3.2	3.9
B90	0.14	0.17	0.23	0.19	B90	3.6	3.2	3.1	3.7
B120	0.16	0.18	0.16	0.17	B120	3.7	2.9	3.3	3.6
B150	0.09	0.20	0.20	0.16	B150	3.4	3.3	3.2	3.5
B180	0.12	0.20	0.15	0.16	B180	4.4	3.3	3.7	3.6
B210	0.15	0.17	0.15	0.18	B210	4.1	3.4	3.5	3.2
B240	0.19	0.15	0.17	0.19	B240	3.6	3.2	3.6	3.9
Blank	0.10	0.10	0.08	0.17	Blank	3.6	3.4	7.1	3.0

in the Day plot probably reflects the presence of a mixture of fine- and coarse-grained ferrimagnetic minerals. The magnetization ratio remains relatively constant in the top part of the palaeosol, and then starts to increase to reach the highest M_{rs}/M_s ratios in the loess. From top to bottom, the coercivity ratio decreases in the top part of the palaeosol and starts to increase in the enhanced lower part of the palaeosol. Going further down, the B_{cr}/B_c ratio decreases again toward the loess.

IRM components

The automated fitting of the isothermal remnant magnetization components (Heslop *et al.* 2002) shows that a two-component IRM yields statistically the best fit for all samples (see Fig. 5 for typical examples throughout the section, panels a–f). One component has a low coercivity (the soft component), and the other has a very high coercivity (the hard component). The relative contribution of the low- and high-coercivity components in the palaeosol samples is ~ 90 and ~ 10 per cent, respectively ($\sim 3.2 \times 10^{-3}$ versus $\sim 0.4 \times 10^{-3} \text{ A m}^2 \text{ kg}^{-1}$, see Table 3). The loess samples have a slightly higher contribution of high-coercivity material, ~ 15 and ~ 85 per cent of low-coercivity material ($\sim 1 \times 10^{-3}$ versus $\sim 0.2 \times 10^{-3} \text{ A m}^2 \text{ kg}^{-1}$, see Table 3).

The low-coercivity component in the palaeosol has a lower $B_{1/2}$ than that of the loess (respectively, ~ 30 and ~ 50 mT), while both components have a similar dispersion of 0.5. The dispersion is given in log-field units, therefore the dispersion of the $B_{1/2}$ of the soft component in the palaeosol is ~ 10 to ~ 93 mT and in the loess this is ~ 16 to ~ 155 mT. This component most probably originates from SD to PSD magnetite. The lower $B_{1/2}$ in the palaeosol compared with that of the loess samples cannot originate from the low-temperature oxidation of magnetite, as this would lead to an increase in coercivity (van Velzen & Dekkers 1999). The difference is probably a result of an increased abundance of finer ferrimagnetic grains including superparamagnetic (SP) grains; this decreases the overall $B_{1/2}$ of the sample, because the coercivity of SP grains is formally zero (Dunlop & Özdemir 1997). Grains that are close to being truly SP will therefore lower the overall $B_{1/2}$ of a sample.

The average $B_{1/2}$ of the high-coercivity component in the palaeosol is ~ 1050 mT with a dispersion of 0.5 ($=316\text{--}3470$ mT). In the loess, the $B_{1/2}$ of the hard component is ~ 500 mT and the dispersion is wider ($0.8 = 79\text{--}3161$ mT). This hard component is either haematite or goethite. The colour of the samples suggests the presence of haematite, but based on colour alone goethite cannot be excluded. The mineralogy was verified with thermal demagnetization of a tri-axial IRM (Lowrie 1990). The saturation IRM of some

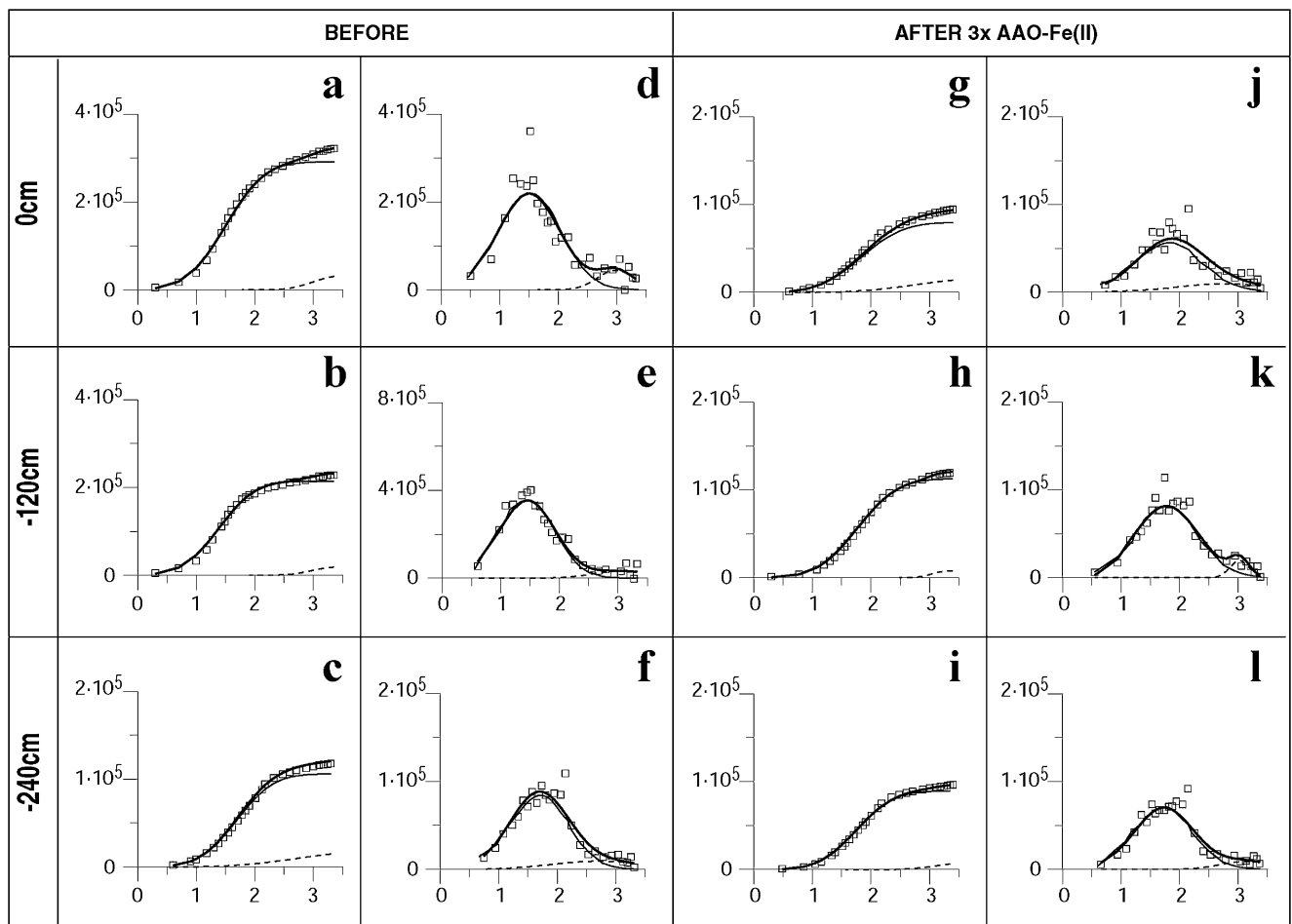


Figure 5. IRM component analysis for some typical palaeosol and loess samples. Data points are indicated by open squares. The sum of all components is represented by a thick black line, the thin solid line represents the soft component and the dashed line represents the hard component. Panels a–c are IRM acquisition curves of unextracted samples, panels g–i represent IRM acquisition curves of the same samples after three AAO- Fe^{2+} extraction steps. Panels d–f and j–l represent the IRM gradient analysis of original and extracted samples, respectively. In all panels the vertical axis represents IRM, while the horizontal axis represents the \log_{10} of the applied field (mT). Before fitting, all data were corrected for the IRM signal and mass of the epoxy resin in each sample.

Table 3. The average values of SIRM ($10^{-8} \text{ A m}^2 \text{ kg}^{-1}$), midpoint $B_{1/2}$ (mT), dispersion (DP) and relative contribution (per cent) of the IRM components in the palaeosol and in the loess samples. The DP is given in log-field values (mT values are given in parentheses). The first values are from unextracted samples, the second set of values are of extracted samples and the final set is from the dissolved fraction (before–after). The average of the palaeosol samples is determined from samples between 0 and -180 cm , while the loess value is determined from samples at -240 cm . The standard deviation of the average samples is given in a smaller font size.

Sample	Component 1				Component 2			
	SIRM	$B_{1/2}$	DP	Contribution	SIRM	$B_{1/2}$	DP	Contribution
Before								
Average soil	321 143	30	0.49 (10–93 mT)	88.6	40 657	1048	0.52 (316–3470 mT)	11.4
	$\pm 76\,500$	± 3	± 0.03	± 3	$\pm 10\,815$	± 455	± 0.14	± 3
Loess	106 000	49	0.50 (16–155 mT)	84.8	19 000	501	0.80 (79–3161 mT)	15.2
After								
Average soil	90 857	58	0.55 (16–206 mT)	84.8	16 000	920	0.52 (278–3046 mT)	15.2
	$\pm 13\,600$	± 5	± 0.02	± 5.6	± 5690	± 331	± 0.27	± 5.6
Loess	90 000	55	0.51 (17–178 mT)	90.0	10 000	1413	0.44 (513–3892 mT)	10
Dissolved								
Average soil	241 571	25	0.46 (9–72 mT)	94.7	13 000	1597	0.33 (747–3414 mT)	5.3
	$\pm 70\,470$	± 1	± 0.01	± 1.8	± 4320	± 369	± 0.09	± 1.8
Loess	22 100	45	0.59 (12–175 mT)	99.1	210	1259	0.18 (832–1906 mT)	0.9

representative samples from the section was split into three orthogonally directed components in the sample. The a -axis contained the hard component with $B_{cr} > 126 \text{ mT}$, the b -axis contained the intermediate component ($30 < B_{cr} < 126 \text{ mT}$) and the c -axis contained the soft component ($B_{cr} < 30 \text{ mT}$). These field values were based on the results of the IRM fit. The values for the hard component are taken rather broadly (there will be a signal from the soft component in this component); however, in this way it is easier to measure changes in the signal, because the hard component has such a weak IRM that it would fall within the error margin of the equipment.

The samples were subsequently thermally demagnetized at 60, 80, 100, 120 and $140 \text{ }^\circ\text{C}$. The decrease in IRM with increasing temperature is gradual for all components (Fig. 6), this indicates that the hard component could not have originated from goethite, which has a Néel temperature of $\sim 120 \text{ }^\circ\text{C}$. An IRM residing in goethite would decay rapidly at low temperatures and show a break in slope at $100\text{--}120 \text{ }^\circ\text{C}$.

FORC distribution

A FORC distribution is a contour plot that allows the user to evaluate magnetic hardness and interaction separately in a sample. The horizontal axis H_c represents the coercivity, and the vertical axis H_u represents the magnetic interaction in the sample (Pike *et al.* 1999). Non-interacting samples have narrow distributions centred on $H_u = 0$. SD particles centre on their H_c , close to the ordinate of the plot they have no contour density (Pike *et al.* 1999; Roberts *et al.* 2000). Modelling has shown that thermal relaxation of SP (and small SD) particles yields vertical contour lines with the maximum contour density at $H_c = 0$ (Pike *et al.* 2001a). Preliminary modelling of MD grains indicate vertical contour lines centred on H_c of the particles (Pike *et al.* 2001b). In practice small MD grains have contour lines shaped like an acute triangle with the base at an angle $\neq 0$ with the horizontal axis ($= \blacktriangleright$) (Roberts *et al.* 2000). The contour density is spread over a comparatively large H_u

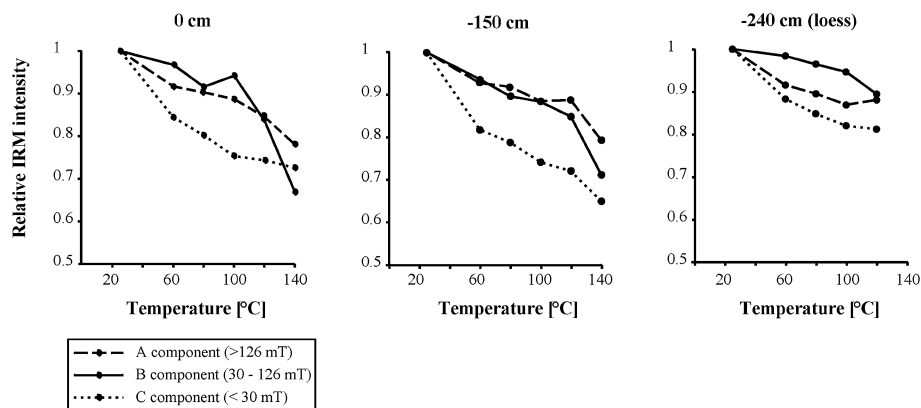


Figure 6. Thermal demagnetization of tri-axial IRM. The two left-hand panels are two palaeosol samples and the right-hand panel is a loess sample. The vertical axis denotes the relative IRM intensity and the horizontal axis shows the temperature steps used for the thermal demagnetization. The $140 \text{ }^\circ\text{C}$ step for the loess samples is not given, the plastic container with the orientation marks which holds the sample, had become partly molten during this final heating step making it impossible to determine the IRM. The dashed line represents the hard component (A), the solid line indicates the intermediate IRM component (B) and the dotted line represents the soft component (C). The intensity of the hard component was the lowest, and that of the soft component was always highest. The initial intensity for the different components in the 0 cm sample was 1410 , 2600 and $3430 \times 10^{-9} \text{ A m}^2$ (A, B and C component, respectively). In the -150 cm sample this was 1240 , 4320 and $5030 \times 10^{-9} \text{ A m}^2$ and in the loess sample (-240 cm) this was 500 , 1090 and $1250 \times 10^{-9} \text{ A m}^2$ (A, B and C, respectively).

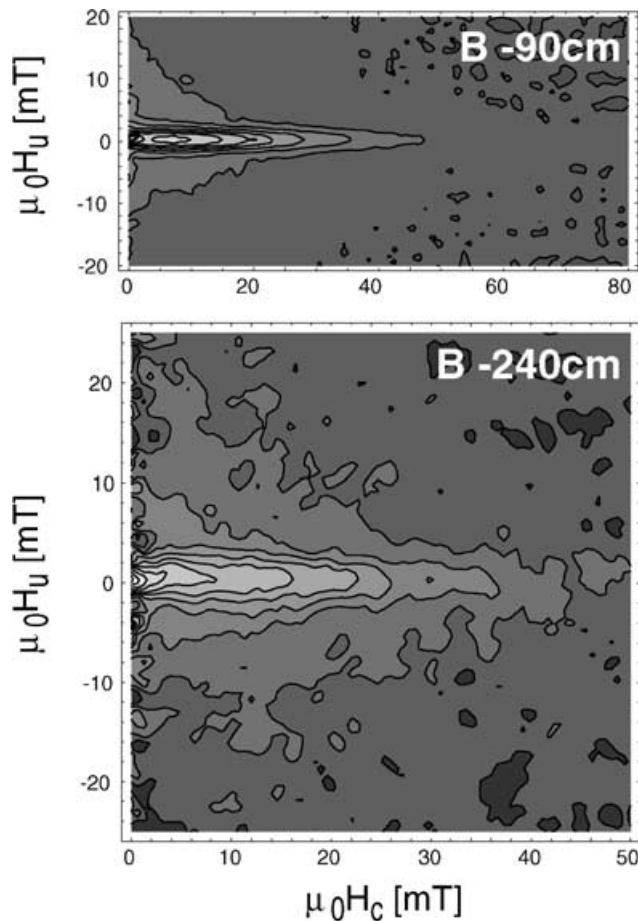


Figure 7. FORC diagram of some representative samples of unextracted bulk material. The horizontal axis denotes $\mu_0 H_c$ (indicative of grain-size range) and the vertical axis represents $\mu_0 H_u$ (indicative of magnetic interaction). The saturation field for both diagrams was 500 mT, and 106 FORC curves were measured. The top diagram is an example from the palaeosol (measurement averaging time of 2 s) and the lower diagram is from the loess horizon (measurement averaging time of 1 s).

interval because the domains within MD particles interact with each other.

The FORC distribution of the palaeosol (Fig. 7 upper panel) and loess (Fig. 7 lower panel) samples indicates dominant fine-grained SD magnetite. In the palaeosol sample the increased contour density close to the ordinate axis might be interpreted as indicative of the presence of SP particles. The triangular shape of the contours indicates the presence of a minor amount of MD grains as well. The wide distribution in coercivity (up to ~ 50 mT), and the narrow vertical distribution (most contours within ± 2 mT) indicate the presence of well-dispersed SD grains. There is no displacement along the vertical axis, confirming that there is little magnetic interaction in the sample.

The loess sample shows slightly larger grains: there are more contours with MD-like triangular shape, and the distribution is somewhat more centred to the left. Also the vertical distribution is more spread out (most contours are within ± 4 mT). The presence of SP grains cannot be evaluated because the weak magnetic signal required a large smoothing factor to produce the FORC diagram shown. This makes the leftmost part of the diagram less reliable. In both palaeosol and loess the magnetic dominance of the magnetite precludes a meaningful determination of high-coercivity components.

Characterization of extracted samples

Low-field susceptibility

In the palaeosol samples, χ_{in} decreased most significantly after one AAO- Fe^{2+} extraction step (Fig. 4). At least part of the magnetic mineral assemblage has been dissolved because the colour of the samples changed from brown-red to beige after extraction, suggesting that (at least part of) the haematite pigment has dissolved. After one extraction the susceptibility varied between $-60 \times 10^{-9} \text{ m}^3 \text{ kg}^{-1}$ for the most enhanced part of the palaeosol, and $\sim -120 \times 10^{-9} \text{ m}^3 \text{ kg}^{-1}$ for the other palaeosol samples and $-140 \times 10^{-9} \text{ m}^3 \text{ kg}^{-1}$ for the loess sample. After two extractions, the bulk susceptibility of all samples remained constant at $-150 \times 10^{-9} \text{ m}^3 \text{ kg}^{-1}$. The data for the blank samples remained constant at $-240 \times 10^{-9} \text{ m}^3 \text{ kg}^{-1}$. χ_{fd} could not be determined for the extracted samples, because low- and high-frequency measurements yielded essentially the same value (the potentially present difference appeared to be below the resolution of the instrument), resulting in a χ_{fd} equal to zero.

In a previous paper (van Oorschot & Dekkers 2001) we have mentioned that pH is important to the AAO- Fe^{2+} treatment because at different pH the dissolution reaction rates distinctly vary. At pH values >4 the dissolution reaction is much slower than that at pH 3–4. In the case of the loess samples, carbonate contents were reasonably high and this carbonate buffered the pH of the extraction solution to values of 5–6. It was only in the last extraction step that pH was in the correct range, i.e. ~ 3 . However, during the whole experiment no prominent change in the magnetic signal of the loess samples occurred (not even in the last extraction step when fast dissolution of iron oxides could take place). Therefore, in the present case, the carbonate content does not affect the outcome of the method.

Hysteresis parameters

A similar change in hysteresis parameters after one extraction step is observed for all palaeosol samples: the coercivity ratio decreases, while the magnetization ratio increases slightly (Table 2). Fig. 8 shows that both B_{cr} and B_c increase after one extraction step. The value of B_c does not change further with more extraction steps and remains at a value of ~ 12 mT. B_{cr} keeps increasing after each extraction step with endvalues of ~ 40 – 50 mT in the palaeosol samples. The coercivity ratio first decreases owing to the relatively fast increase in B_c compared with B_{cr} , but the stabilization of B_c after one extraction step causes the coercivity ratio to start increasing again. The magnetization ratio increased slightly, with the most noticeable increase in magnetization ratio being for the most enhanced part of the palaeosol (Fig. 8). The increase in magnetization ratio is related to the strong decrease in M_s of all samples except for the loess samples. After one extraction step, the palaeosol samples have lost 50–80 per cent of their original M_s . More extraction steps hardly affect the M_s and it remains at $\sim 1 \times 10^{-2} \text{ A m}^2 \text{ kg}^{-1}$, similar to the M_s of the loess samples and the quartz blanks. M_{rs} also decreases less rapidly in the second and third extraction step, which causes the magnetization ratio to stabilize at a slightly higher value than that of the original samples.

The samples in the lower part of the section (loess and transition from palaeosol to loess) behave differently, here B_{cr} hardly changes with extraction and the coercivity ratio remains constant. The M_s decreases slightly in the loess samples but the magnetization ratio remains constant. The loess samples show a decrease in both magnetization and coercivity ratio. The samples have very similar B_{cr} and M_s to the quartz blanks, which could indicate that all iron oxides

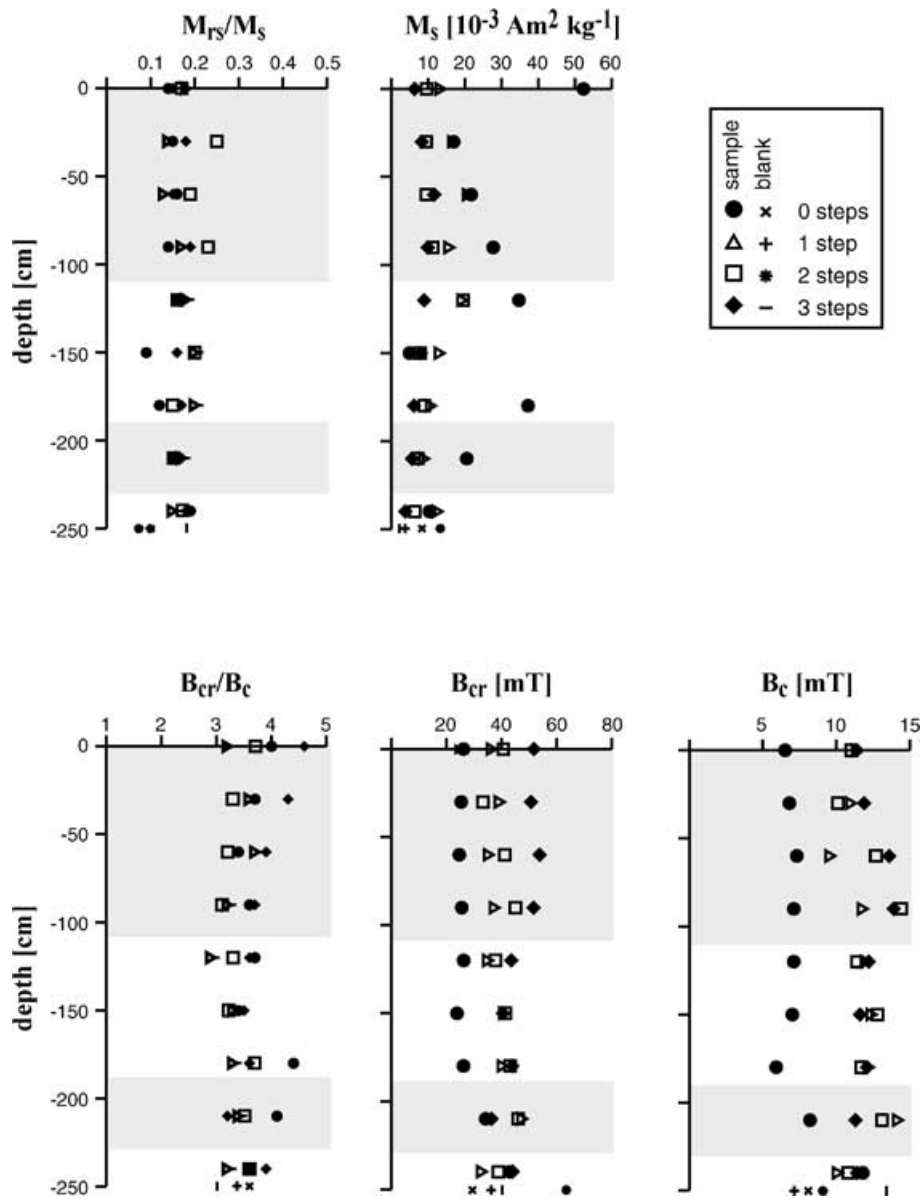


Figure 8. Change in hysteresis parameters (M_{rs}/M_s , M_s , B_{cr}/B_c , B_c and B_{cr}) with depth of the section as well as with each extraction step. Closed circles represent the non-extracted samples and closed diamonds represent the same samples after three extraction steps. The open triangles and squares are from extraction step 2 and 3, respectively.

have been removed from the sample (which was confirmed visually by the change in colour from brown–red to beige), but B_c is slightly higher than that of the blanks.

IRM components

After extraction, all samples still have a two-component IRM distribution (Fig. 5, panels g–l). In the palaeosol samples the relative contribution of the components has changed to ~ 85 per cent for the soft component and ~ 15 per cent for the hard component ($\sim 9 \times 10^{-4}$ versus $\sim 1.6 \times 10^{-4}$ A m² kg⁻¹, see Table 3). This indicates that the soft component has been preferentially dissolved from the soil samples. The soft component in all palaeosol samples has an average $B_{1/2}$ value of ~ 58 mT, and the hard component has a decreased $B_{1/2}$ value of ~ 900 mT. Both components in the palaeosol samples have dispersions of ~ 0.5 (component 1, 16–206 mT; component 2, 278–3046 mT).

The relative contribution of the soft component has increased in the loess samples (~ 90 per cent or 9×10^{-4} A m² kg⁻¹), while the contribution of the hard component has decreased (~ 10 per cent or 1×10^{-4} A m² kg⁻¹). The average $B_{1/2}$ of the soft component in the loess is ~ 55 mT with a dispersion of 0.51 (17–178 mT), the hard component has an increased $B_{1/2}$ value of ~ 1400 mT and has a more narrow dispersion of 0.44 (513–3892 mT).

The dissolved magnetic fraction is represented in the curve of the difference in IRM acquisition between the original and the extracted samples (Fig. 9). Analysis of these curves shows that mainly the soft component dissolved during the extraction. The magnetic contribution of the soft component to the dissolved fraction is ~ 95 per cent (2.4×10^{-3} A m² kg⁻¹) in the average of the palaeosols (seven samples) and even ~ 99 per cent in the loess samples (2.2×10^{-4} A m² kg⁻¹). The $B_{1/2}$ of the dissolved soft component is 25 mT in the palaeosol samples, and 45 mT in the loess (dispersions are 0.46

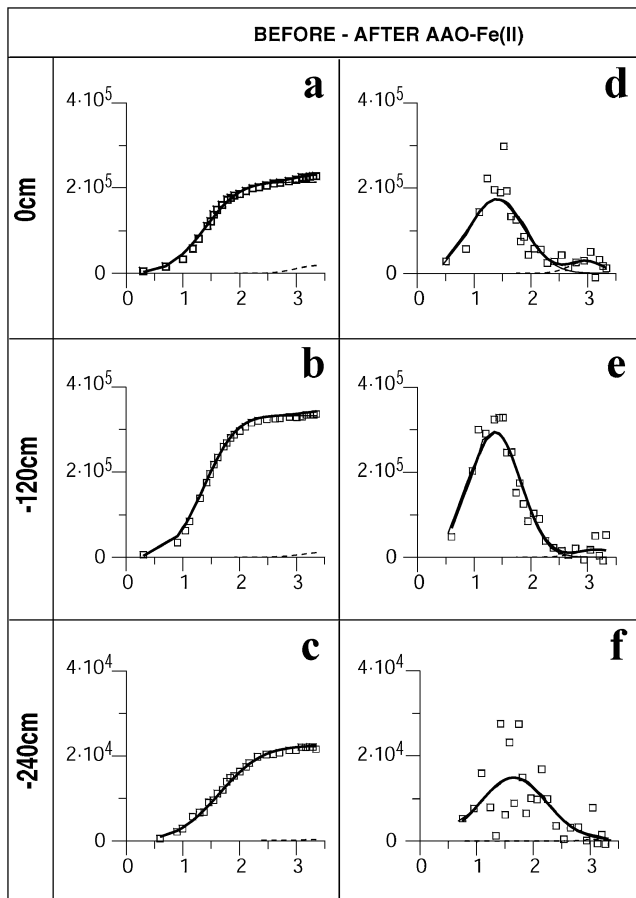


Figure 9. IRM component analysis for the difference in IRM acquisition before and after extraction for some typical palaeosol and loess samples. Data points are indicated by open squares. The sum of all components is represented by a thick black line, the thin solid line represents the soft component and the dotted line represents the hard component. Panels a–c are IRM acquisition curves and panels d–f represent the IRM gradient analysis of the subtracted data set. In all panels the vertical axis represents IRM, while the horizontal axis represents the \log_{10} of the applied field (mT). Before fitting, all data were corrected for the IRM signal and the mass of the epoxy resin in each sample.

(or 9–72 mT) and 0.59 (or 12–175 mT), respectively). The $B_{1/2}$ of the dissolved hard component is ~ 1600 mT in the palaeosol samples, and ~ 1250 mT in the loess (dispersions are 0.33 (or 747–3414 mT) and 0.18 (or 832–1906 mT), respectively). Of the total amount of dissolved iron oxides, only 1–5 per cent of the hard component has dissolved from the loess and the palaeosol samples, respectively (2×10^{-6} and 1.3×10^{-4} A m² kg⁻¹, see Table 3). It seems that the loss in magnetic particles is most probably related to dissolution of newly formed (very fine-grained) pedogenic iron oxides (such as the haematite pigment and SP-like ferrimagnetic particles) as well as the dissolution of the weathered surface of coarse-grained ferrimagnetic particles in the loess. Because of the difference in magnetic characteristics between magnetite and haematite it is difficult to judge whether one or the other was dissolved preferentially. Most of the magnetically enhanced signal stems from fine-grained magnetite. After extraction it was by and large removed; however, because magnetite is so much more magnetic than haematite, on a molar basis most of the dissolved minerals probably came from haematite and not from magnetite.

FORC distribution

The FORC diagrams of the extracted samples show a pattern with a wider vertical distribution (with a maximum of 40 mT) but no vertical displacement of the centre of distribution (Fig. 10). The magnetic signal was weak, requiring rather high smoothing factors to produce the plots shown. It is remarkable that the coercivity contour distribution along the horizontal axis goes up to values of ~ 80 mT (before extraction this was up to ~ 50 mT), this could suggest the presence of high-coercivity material. The FORC diagrams, with their increased triangular shape, thus show an increase in MD character after extraction, with increased magnetic (intraparticle) interaction. The wider distribution of coercivities may be caused by the dissolution of magnetite during the extraction experiments. The partial disappearance of the SD magnetite signal facilitates the expression of the weakly magnetic haematite.

DISCUSSION AND CONCLUSIONS

The normal polarity of all samples indicates that the section was formed during the Brunhes; the pedocomplex assignment precludes

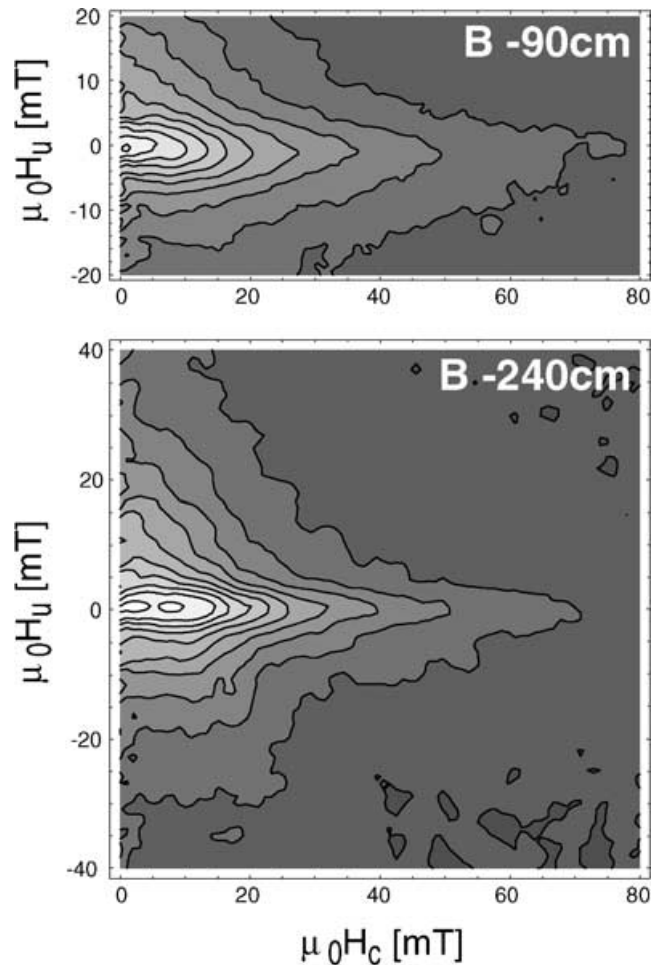


Figure 10. FORC diagram of some representative samples after three AAO-Fe²⁺ extraction steps. The horizontal axis denotes $\mu_0 H_c$ and the vertical axis represents $\mu_0 H_u$. The saturation field for both diagrams was 500 mT, and 106 FORC curves were measured. The measurement averaging time was 2 s. The top diagram is an example from the palaeosol and the lower diagram is from the loess horizon.

formation during the Jaramillo subchron. Viscous resetting of the NRM is unlikely, because the declinations in particular deviate from the geocentric axial dipole direction for the site. The higher NRM intensity of the palaeosol samples is consistent with its enhanced susceptibility, indicating that the enhancement originates from an increased concentration of ferrimagnetic particles in the palaeosol. In the top of the palaeosol, most of the NRM is lost after applying a field of only ~ 40 mT, indicating that the main carrier of the magnetic signal in the top of the palaeosol is a ferrimagnetic mineral (most probably magnetite, as $T_C = 590$ °C) of small SD or PSD/MD size. The high χ_{fd} pleads for the former. In the more enhanced part of the palaeosol (between -50 and -165 cm) as well as in the loess, most of the NRM is lost after applying a field of 80 – 100 mT, indicative of SD to PSD size magnetite. Here, the hysteresis parameters are plotted in the PSD region as well. The high-coercivity component determined by the IRM component analysis does not emerge in the NRM behaviour.

IRM component analysis shows that all samples contain a two-component IRM. The low-coercivity component is interpreted to be SD magnetite, and the high-coercivity component originates from haematite. The higher value of $B_{1/2}$ and narrow dispersion of the hard component in the palaeosol compared with that in the loess, indicates neof ormation of fine-grained haematite in the former. This is confirmed by the higher intensity of NRM in the palaeosol samples after demagnetization to 250 mT (which is 4 – 10 times higher in the palaeosol samples than in the loess samples).

The FORC diagrams follow the pattern of the soft IRM component and display predominantly well-dispersed SD magnetite. However, the presence of haematite can be inferred from the fairly high coercivity values found in FORC diagrams of AAO-Fe²⁺-treated samples.

After AAO-Fe²⁺ treatment, the susceptibility in all samples has decreased except for the loess samples, and the decrease was strongest after one extraction step. The loess samples were hardly affected—this was not related to the high carbonate content. The susceptibility of the palaeosol samples after extraction was comparable with that of the loess samples. From the second extraction step onward, palaeosol and loess samples behaved along similar lines. Therefore, all pedogenic iron oxides have probably been removed from the samples during the first extraction step, which is confirmed by the change in colour from brown–red to beige. Also, the AAO-Fe²⁺ extraction method has not affected the coarser lithogenic particles in the samples, a behaviour that concurs with the results obtained for synthetic samples (van Oorschot & Dekkers 2001).

The hysteresis parameters confirm that predominantly small SP/SD grains were removed by the extraction method (the magnetization ratio increased, while the coercivity ratio decreased). The loess samples have lost some SD grains (both magnetization and coercivity ratios decreased). The dissolution of fine-grained magnetite was also detected with the IRM component analysis. After extraction, the relative contribution of lithogenic haematite to the IRM signal of the palaeosol had increased, indicating that the soft component had been preferentially removed.

The loess samples also lost part of the haematite during extraction, as indicated by the decrease in dispersion and the absolute IRM contribution of the hard component. The FORC diagrams of extracted samples all showed an increase in MD character, as demonstrated by an increased magnetic (intraparticle) interaction. The SP/SD material had been removed from the samples which is in agreement with the example shown by Roberts *et al.* (2000) for the CBD extraction. χ_{fd} of the samples after extraction unfortunately fell below the

resolution of the instrument, thus precluding confirmation by χ_{fd} behaviour.

It is shown here that the AAO-Fe²⁺ extraction technique is expected to dissolve fine-grained (SP/SD) ferrimagnetic minerals as well as pedogenic haematite from palaeosol samples in one extraction step. Magnetically speaking, the method preferentially attacked the magnetite grains, however, since haematite is magnetically much weaker, in fact more haematite was removed than magnetite. This method is slightly less aggressive than the CBD method and offers better discrimination in the ultrafine grain-size range. The relative stability of the magnetic parameters in the loess before and after extraction supports this discrimination. The method has successfully dissolved the pedogenic components from the palaeosol samples.

ACKNOWLEDGMENTS

The authors greatly appreciated the help of all participants in the field trip to Moravia, and would especially like to thank Adry van Velzen, Neli Jordanova and Eduard Petrovsky. The authors also wish to thank Pauline Kruiver and David Heslop for their assistance with the IRM component analysis as well as for fruitful discussions of the results. The help of Chris Pike with the FORC analysis was greatly appreciated. This work was conducted under the programme of the Vening Meinesz Research School of Geodynamics (VMSG), and funded by the Netherlands Organization for Scientific Research (NWO/ALW).

REFERENCES

- Busacca, A.J., 1989. Long Quaternary record in eastern Washington, USA, interpreted from multiple buried palaeosols in loess, *Geoderma*, **45**, 105–122.
- Cornell, R.M. & Schwertmann, U., 1996. *The Iron Oxides*, p. 573, VCH, Weinheim.
- Day, R., Fuller, M. & Schmidt, V.A., 1977. Hysteresis properties of titanomagnetites: grain-size and compositional dependence, *Phys. Earth planet. Inter.*, **13**, 260–266.
- Dunlop, D.J. & Özdemir, Ö., 1997. *Rock Magnetism: Fundamentals and Frontiers*, p. 573, Cambridge University Press, Cambridge.
- Fang, X.-M. *et al.*, 1999. Asian summer monsoon instability during the past 60 000 years: magnetic susceptibility and pedogenic evidence from the western Chinese Loess Plateau, *Earth planet. Sci. Lett.*, **168**, 219–232.
- Frechen, M., Zander, A., Cilek, V. & Lozek, V., 1999. Loess chronology of the last interglacial/glacial cycle in Bohemia and Moravia, Czech Republic, *Quaternary Sci. Rev.*, **18**, 1467–1493.
- Hanesch, M. & Petersen, N., 1999. Magnetic properties of a recent parabrown-earth from Southern Germany, *Earth planet. Sci. Lett.*, **169**, 85–97.
- Havlicek, P. & Smolikova, L., 1993. A loess series near Boretice (South Moravia), *Bull. Czech Geol. Survey*, **68**, 19–24.
- Heller, F. & Evans, M.E., 1995. Loess magnetism, *Rev. Geophys.*, **33**, 211–240.
- Heller, F. & Liu, T.-S., 1986. Palaeoclimatic and sedimentary history from magnetic susceptibility of loess in China, *Geophys. Res. Lett.*, **13**, 1169–1172.
- Heslop, D., Langereis, C.G. & Dekkers, M.J., 2000. A new astronomical timescale for the loess deposits of Northern China, *Earth planet. Sci. Lett.*, **184**, 125–139.
- Heslop, D., Dekkers, M.J., Kruiver, P.P. & van Oorschot, I.H.M., 2002. Analysis of isothermal remanent magnetisation acquisition curves using an expectation–maximisation algorithm, *Geophys. J. Int.*, **148**, 58–64.

- Hunt, C.P., Singer, M.J., Kletetschka, G., TenPas, J. & Verosub, K.L., 1995. Effect of citrate–bicarbonate–dithionite treatment on fine-grained magnetite and maghemite, *Earth planet. Sci. Lett.*, **130**, 87–94.
- Kletetschka, G. & Banerjee, S.K., 1995. Magnetic stratigraphy of Chinese loess as a record of natural fires, *Geophys. Res. Lett.*, **22**, 1341–1343.
- Kraus, M.J., 1999. Paleosols in clastic sedimentary rocks: their geologic applications, *Earth Sci. Rev.*, **47**, 41–70.
- Kruiver, P.P., Dekkers, M.J. & Heslop, D., 2001. Quantification of magnetic coercivity components by the analysis of acquisition curves of isothermal remnant magnetisation, *Earth planet. Sci. Lett.*, **189**, 269–276.
- Kukla, G.J., 1987. Loess stratigraphy in central China, *Quaternary Sci. Rev.*, **6**, 191–219.
- Kukla, G.J., Heller, F. & Xu, T.-C., 1990. Frequency-dependent susceptibility of loess and Quaternary climate, *Quaternary Sci.*, **3**, 42–50.
- Kuntze, H., Niemann, J., Roeschmann, G. & Schwerdtfeger, G., 1981. *Bodenkunde*, 2nd edn, p. 407, Eugen Ulmer, Stuttgart.
- Liu, X.M., Hesse, P., Liu, T.S. & Bloemendal, J., 1998. High resolution climate record from the Beijing area during the last glacial–interglacial cycle, *Geophys. Res. Lett.*, **25**, 349–352.
- Lowrie, W., 1990. Identification of ferromagnetic minerals in a rock by coercivity and unblocking temperature properties, *Geophys. Res. Lett.*, **17**, 159–162.
- Maher, B.A., 1998. Magnetic properties of modern soils and Quaternary loessic paleosols: paleoclimatic implications, *Palaeogeog. Palaeoclimat. Palaeoecol.*, **137**, 25–54.
- Pike, C.R., Roberts, A.P. & Verosub, K.L., 1999. Characterizing interactions in fine magnetic particle systems using first order reversal curves, *J. Appl. Phys.*, **85**, 6660–6667.
- Pike, C.R., Roberts, A.P. & Verosub, K.L., 2001a. FORC diagrams and thermal relaxation effects in magnetic particles, *Geophys. J. Int.*, **145**, 721–730.
- Pike, C.R., Roberts, A.P., Verosub, K.L. & Dekkers, M.J., 2001b. An investigation of multi-domain hysteresis mechanisms using FORC diagrams, *Phys. Earth planet. Inter.*, **126**, 13–28.
- Roberts, A.P., Pike, C.R. & Verosub, K.L., 2000. First-order reversal curve diagrams: a new tool for characterising the magnetic properties of natural samples, *J. geophys. Res.*, **105**, 28 461–28 475.
- Sartori, M., Heller, F., Forster, T., Borkovec, M., Hammann, J. & Vincent, E., 1999. Magnetic properties of loess grain size fractions from the section at Paks (Hungary), *Phys. Earth planet. Inter.*, **116**, 53–64.
- Singer, M.J. & Fine, P., 1989. Pedogenic factors affecting magnetic susceptibility of Northern California soils, *Soil Sci. Soc. Am. J.*, **53**, 1119–1127.
- Singer, M.J., Bowen, L.H., Verosub, K.L., Fine, P. & TenPas, J., 1995. Mössbauer spectroscopic evidence for citrate–bicarbonate–dithionite extraction of maghemite from soils, *Clays Clay Minerals*, **43**, 1–7.
- Stremme, H.E., 1998. Correlation of Quaternary pedostratigraphy from western to eastern Europe, *Catena*, **34**, 105–112.
- Thompson, R. & Oldfield, F., 1986. *Environmental Magnetism*, p. 227, Allen & Unwin, London.
- van Oorschot, I.H.M. & Dekkers, M.J., 1999. Dissolution behaviour of fine-grained magnetite and maghemite in the citrate–bicarbonate–dithionite extraction method, *Earth planet. Sci. Lett.*, **167**, 283–295.
- van Oorschot, I.H.M. & Dekkers, M.J., 2001. Selective dissolution of magnetic iron oxides in the acid-ammonium-oxalate/ferrous-iron extraction method—I. Synthetic samples, *Geophys. J. Int.*, **145**, 740–748.
- van Velzen, A.J. & Dekkers, M.J., 1999. Low-temperature oxidation of magnetite in loess-paleosol sequences: a correction of rock magnetic parameters, *Studia Geophys. Geod.*, **43**, 357–375.
- Zhou, L.P. & Shackleton, N.J., 1999. Misleading positions of geomagnetic reversal boundaries in Eurasian loess and implications for correlation between continental and marine sedimentary sequences, *Earth planet. Sci. Lett.*, **168**, 117–130.